Bioinspiration & Biomimetics

RECEIVED
20 December 2016

REVISED
10 April 2017

ACCEPTED FOR PUBLICATION
12 April 2017

PUBLISHED
19 May 2017

PAPER

Detection of magnetic field properties using distributed sensing: a computational neuroscience approach

Brian K Taylor[1,4], **Sönke Johnsen**[2] **and Kenneth J Lohmann**[3]

[1] Integrated Sensing and Processing Sciences, Air Force Research Laboratory—Munitions Directorate, Eglin Air Force Base, Florida, United States of America
[2] Department of Biology, Duke University, Durham, North Carolina, United States of America
[3] Department of Biology, University of North Carolina at Chapel Hill, Chapel Hill, North Carolina, United States of America
[4] Author to whom any correspondence should be addressed.

E-mail: brian.taylor.48@us.af.mil, sjohnsen@duke.edu and klohmann@email.unc.edu

Keywords: magnetoreception, animal magnetic reception, dynamic neural fields, computational neuroscience, distributed sensing, navigation, magnetosensing

Abstract

Diverse taxa use Earth's magnetic field to aid both short- and long-distance navigation. Study of these behaviors has led to a variety of postulated sensory and processing mechanisms that remain unconfirmed. Although several models have been proposed to explain and understand these mechanisms' underpinnings, they have not necessarily connected a putative sensory signal to the nervous system. Using mathematical software simulation, hardware testing and the computational neuroscience tool of dynamic neural fields, the present work implements a previously developed conceptual model for processing magnetite-based magnetosensory data. Results show that the conceptual model, originally constructed to stimulate thought and generate insights into future physiological experiments, may provide a valid approach to encoding magnetic field information. Specifically, magnetoreceptors that are each individually capable of sensing directional information can, as a population, encode magnetic intensity and direction. The findings hold promise both as a biological magnetoreception concept and for generating engineering innovations in sensing and processing.

1. Introduction

Several animals use Earth's magnetic field as a part of their navigation toolset to accomplish tasks ranging from local homing to long-distance migration on the scale of ocean basins ((Wiltschko and Wiltschko 1995, Johnsen and Lohmann 2005, 2008) and the 2010 special edition on magnetosensing by the *Journal of the Royal Society: Interface*). Earth's magnetic field is a three-dimensional vector field that extends from the planet's surface up through the atmosphere. One way to describe the magnetic field is by its intensity (i.e. vector magnitude), inclination angle (i.e. angle between the magnetic field vector and the local horizontal plane), and declination angle (i.e. difference between magnetic and geographic north) (Knecht and Shuman 1985, Wajnberg *et al* 2010). An illustration of Earth's magnetic field is shown in figure 1(a).

The intensity of Earth's magnetic field varies predictably across the surface of the globe ((Gould 1982, Skiles 1985) and figure 2). In principle, animals that migrate long distances might therefore derive positional information from spatial variations in field intensity (Lohmann *et al* 1999, 2007). Direct experimental evidence has demonstrated that several animals, including sea turtles (Lohmann and Lohmann 1996) and salmon (Putman *et al* 2014), detect magnetic field intensity and use it as a source of positional information in 'magnetic maps'. Such maps can be used by long-distance migrants to steer themselves along migratory pathways or to navigate toward specific target areas (Boles and Lohmann 2003, Lohmann *et al* 2004, 2012). In addition, several other methods of navigation that rely at least partly on detecting magnetic field intensity have been proposed in hammerhead sharks (Klimley 1993), pigeons (Walker 1998, Dennis *et al* 2007) and whales (Klinowska 1985, Kirschvink *et al* 1986).

Although at least some animals can clearly detect magnetic field intensity, how they do so has remained enigmatic. Several attempts to approach the problem of intensity detection from a theoretical perspective have assumed that the primary receptors for detecting magnetic fields are crystals of the mineral magnetite (Johnsen and Lohmann 2005, 2008, Shaw *et al* 2015). Some studies have further postulated that multiple sensors that encode direction can simultaneously be used

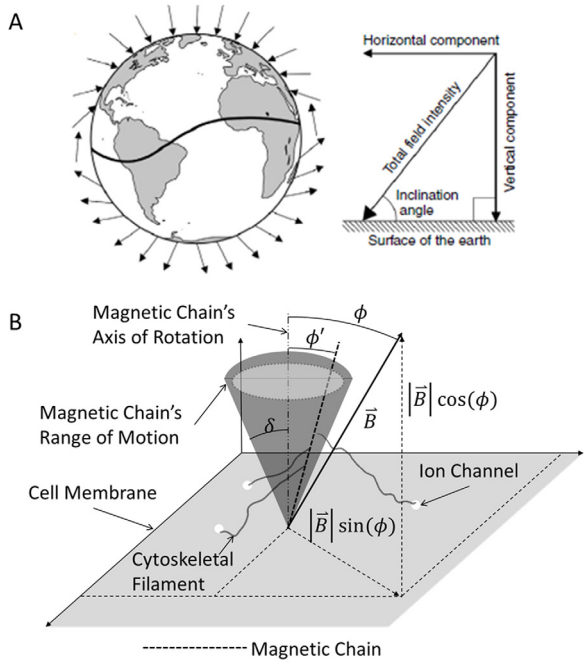

Figure 1. (a) Illustration of Earth's magnetic field. Magnetic field vectors point away from Earth in the Southern Hemisphere, are tangential to Earth at the magnetic equator and point towards Earth in the Northern Hemisphere (reproduced with permission from Lohmann (2007)). (b) Illustration of the Walker (2007) model. A magnetically sensitive chain (the thick dotted line) is connected to mechanically gated ion channels (white circles) on a cell's membrane (gray plane) via cytoskeletal filaments. Because of the chain's mechanical connections, its angular motion ϕ' is restricted to a cone whose half-angle is δ. An external magnetic field $\vec{B}$ causes the chain to change its orientation and frequency of motion. $|\vec{B}|$ represents the magnitude of the magnetic field. $|\vec{B}|\cos(\phi)$ and $|\vec{B}|\sin(\phi)$ represent the components of the magnetic field that are perpendicular and tangential to the cell, respectively.

to encode intensity, because the variance in direction encoded by the sensor population should decrease with increasing field strength (e.g. Yorke (1985), Kirschvink and Walker (1985) and Walker (2007)). While several researchers have taken steps that either observe or catalog how this type of mechanism might work at the neural and cellular levels (Wu and Dickman 2012, Eder *et al* 2012, Wiltschko and Wiltschko 2013, Shaw *et al* 2015, Vidal-Gadea *et al* 2015), it is still an open research area (Edelman *et al* 2015).

Walker (2007) proposed a conceptual model for how a magnetite-based receptor might encode magnetic intensity based on distributed detection of magnetic field direction amongst a population of cells (figure 1(b)). The model proposes that a magnetite chain is anchored to a cell membrane and connected to mechanically gated ion channels by various cellular structures (e.g. cytoskeletal filaments). The membrane's connections restrict the chain's motion to a cone. The presence of a magnetic field that has a particular intensity and orientation relative to the cell will cause the magnetic chain to move with a given set of motion properties, such as a dominant frequency and amplitude. This motion would give rise to ion channel activity. Different magnetic intensities and directions give rise to different chain motion profiles and, by extension, different levels of ion channel activity. Variable ion channel activity provides a mechanism by which a cell can alter its membrane potential over time and thus encode information about the magnetic intensity and direction. By amalgamating the membrane potential changes from cells whose orientations are distributed over three dimensions and accounting for the spatial distribution of cell activity (i.e. which cells are most and least active), the intensity and direction of the magnetic field can be encoded (see figure 3(b) for an illustration). In essence, this model proposes that the magnetic field is encoded via distributed mechanoreception (Zill *et al* 2004, Dargahi and Najarian 2004), which is plausible because magnetoreception might take place within a volume of tissue (Johnsen and Lohmann 2005). Walker's model makes several predictions:

1. Each receptor has a direction of greatest and least response to a given magnetic intensity (i.e. a preferred direction).
2. Rotating (rather than reversing) the field relative to a given cell's preferred direction without changing its intensity may be sufficient to change that cell's membrane potential, similar to what one might observe with an intensity change.
3. A given cell has a minimum threshold of detectable intensity.
4. The mechanism follows Weber's law, which states that the ratio of the change in stimulus (ΔI) to the actual stimulus (I) remains constant. Weber's law is mathematically expressed as $\Delta I = kI$, where k is the Weber fraction. Later works have shown that for a number of sensor modes, perceived stimulus varies with the actual stimulus as either a logarithmic, or power

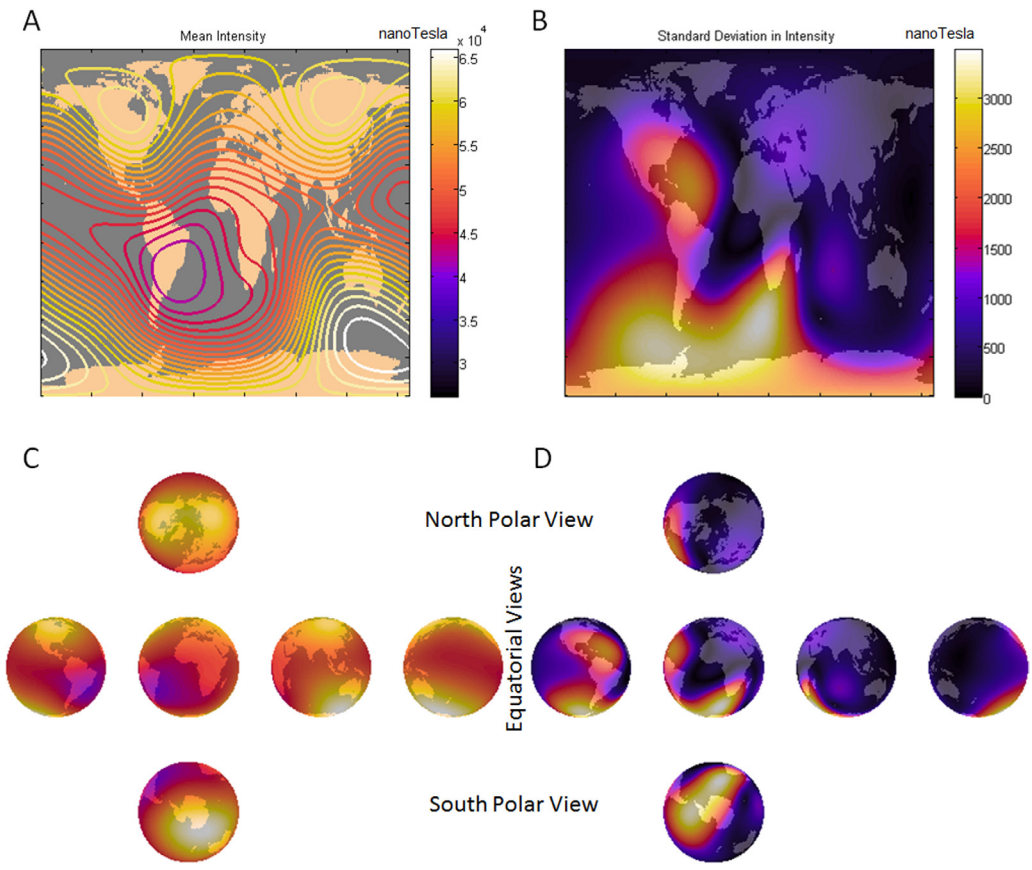

Figure 2. (a) Contour plot of the mean magnetic field intensity from the years 1916–2015. (b) Heat map of the standard deviation in mean intensity. (c) Heat map of the mean intensity superimposed on a globe. (d) Heat map of the standard deviation in intensity superimposed on a globe. Numerical scales for all panels are in nanoTesla. The globes are rotated to six different orientations to show four equatorial views and views of the north and south poles. Also, continent contour data is taken from MATLAB's 'topo.mat' data file, while intensity data was taken from the International Geomagnetic Reference Field (IGRF) model. Panels A and B are plotted in with an equirectangular map projection.

(which includes linear) relationship (Kandel and Schwartz 1981, Shepherd 1994, Kandel *et al* 2000, Akre and Johnsen 2014).

Walker's model provides a plausible explanation of how magnetite-based magnetoreceptors might detect magnetic field intensity. It also provides guidance on possible future physiological experiments and is consistent with magnetite-based magnetoreception studies (Jensen 2010, Wu and Dickman 2012, Eder *et al* 2012, Shaw *et al* 2015). A recent study by Taylor (2016) implemented Walker's conceptual model in a software simulation using computational neuroscience. In particular, by analyzing the response of a simulated dynamic neural field (see section 2.1) to varying magnetic field intensities and directions, the study generated results that supported the predictions of Walker (2007).

The present study attempts to further validate Walker's conceptual model by expanding the work of Taylor (2016) to include both software simulation and hardware experiments. Both simulated and real-world distributed magnetic field data were generated and then processed using the computational neuroscience tool of dynamic neural fields (Trappenberg 2010, Coombes *et al* 2014). Using this approach, the present study suggests that the Walker (2007) model can encode magnetic intensity and direction. Specifically, a unidirectional sensor array can encode intensity on its own, while several unidirectional arrays with different spatial orientations (i.e. a multidirectional sensor array) are able to encode both magnetic intensity and direction (figure 3(b)). Our results support several of the predictions made by Walker (2007), confirm the work of Taylor (2016), provide a tool that can be used to advance biological magnetoreception work and provide insights into processing distributed sensor data in engineered systems.

2. Methods

Detailed methods and mathematics of the current work are described in Taylor (2016) and Taylor and Rutkowski (2015). For brevity, details specific to the current study are presented here, whereas the more detailed mathematics are described in Taylor (2016).

2.1. Dynamic neural fields overview

Dynamic neural fields were used to process magnetic field information. Dynamic neural fields are a computational neuroscience tool that has been developed and used to understand vertebrate sensory processing and nervous

system organization (Wilson 1999, Trappenberg 2010, Coombes *et al* 2014). An example of a neural field approach is a winner-take-all network that can sum vectors, an important ability for tasks such as motor control, motion perception and path integration (Wilson 1999). Modeled after some of the fundamental dynamics of individual neuron models, such as the leaky integrate-and-fire (LIF) neuron (Trappenberg 2010), neural fields have been used to model and study brain organization and sensory processing in a number of areas including motion perception and direction representation (Wilson and Cowan 1973, Wilson 1999, Zhang 1996, Trappenberg 2010, Coombes *et al* 2014). Additionally, they have been used to develop processing architectures and controllers for engineered systems (Browning *et al* 2009, Boxerbaum 2012). Neural fields treat the collective activity and interactions of neurons as a continuum to avoid computational expense. This is in contrast to focusing on the dynamics of, and interactions between, individual neurons, which are important for studying the detailed functionality of small neural circuits, or interactions between a limited number of neurons (e.g. Szczecinski (2013) and Szczecinski *et al* (2013)). Detailed information on different mathematical formulations and properties of dynamic neural fields can be found in Coombes *et al* (2014), Wilson and Cowan (1973), Wilson (1999), Trappenberg (2010), Grossberg (1973) and Amari (1977). The current work advances previous applications of neural fields to magnetoreception (Taylor and Rutkowski 2015, Taylor 2016).

Figure 3(a) illustrates the neural field approach. Several nodes, each representing a neural population or pool sensitive to a particular input, are connected to each other via synaptic weights that excite near neighbors (i.e. local excitation), while inhibiting more distant neighbors (i.e. global inhibition). When the network is stimulated by an input, this local cooperation and global competition between the nodes results in an output signal in which a subset of populations is most active. The output distribution can be used to gain information about the input stimulus (gray arrows of figure 3(a) and all plots of figure 5). Our formulation uses a so-called transient network based on the formulation of Trappenberg (2010) and implementations of Taylor and Rutkowski (2015) and Taylor (2016). A transient network responds in the presence of an input stimulus and then reverts to its baseline activity when the stimulus is removed. Our software simulation used 24 nodes for both the multidirectional and unidirectional sensor arrays. The hardware experiments used eight nodes for the unidirectional array and 64 nodes for the multidirectional array (see section 2.2 for a description of physical sensor layout). Details on the neural field implementation used in this study can be found in Taylor (2016).

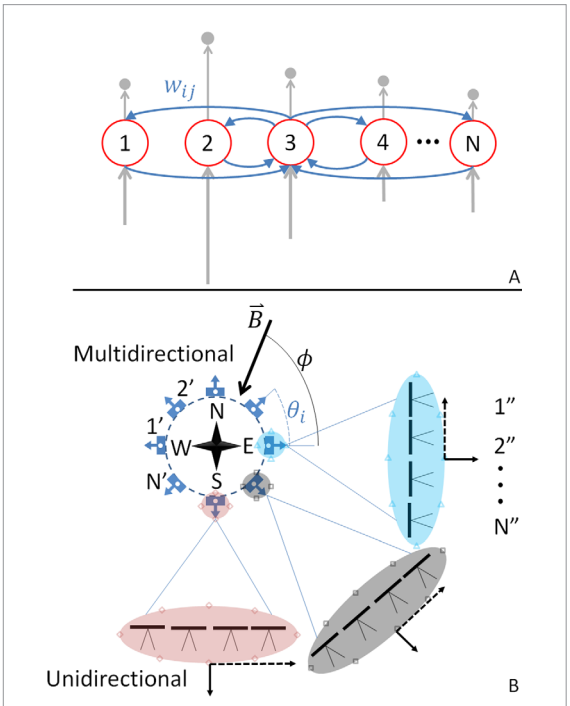

Figure 3. (a) Illustration of dynamic neural fields as used in the present work. The weights w_{ij} represent synaptic connections from neural population i to neural population j. The input stimulus to the neural field is denoted by arrows on the bottom of the network, while the neural field's output is denoted by the arrows connected to the circles on the top of the network. For clarity, only the connections to and from the central node are shown. In reality, each of the nodes could be connected to any combination of other nodes and the network could be fully connected. Also, in general, there could be several sets of populations that interact with one another. (b) Illustration of a ring of magnetically sensitive sensors (i.e. multidirectional array) that are all oriented differently along different preferred directions. When a magnetic field is applied, the sensors will all respond differently due to their different orientations relative to the field. The magnified portions in blue surrounded by triangles, grey surrounded by squares and red surrounded by diamonds illustrate the Walker model as a subpopulation of the magnetically sensitive ring (i.e. unidirectional sensor array). Each element in the subpopulation represents the cell membrane and cone of figure 1. The solid filled black arrows represent the preferred directions of the unidirectional sensor arrays.

2.2. Magnetic field sensors

Sensor data was obtained from both a simulated sensor model and a real-world instantiation of the simulated model (i.e. a hardware model). For both the simulated and hardware sensors, both multidirectional and unidirectional sensor arrays were used (figure 3(b)). In the sensor layouts shown in figure 3(b), only the relative orientation of, and physical connections between, constituent sensors and neural pools matter. The geometric configuration is not important (Zhang 1996). For example, the sensors in the unidirectional array of figure 3(b) could be arranged in a circle, or some other regular or irregular shape. As long as they have the same physical orientations relative to each other and have the same neural connectivity, the results would be the same. For simplicity, we assume that the sensors do not affect the magnetic field and, by extension, the readings of other sensors.

For the simulated sensor arrays, the magnetic field intensity was varied by altering parameters denoted as $\lambda_1|\vec{B}|$ and $\lambda_2|\vec{B}|$. $|\vec{B}|$ represents the intensity of the

magnetic field. λ_1 and λ_2 are parameters that scale the magnetic field intensity in the multidirectional and unidirectional arrays, respectively. The scaling parameters are used to physically relate the magnetic field intensity to properties that are relevant to a cell, such as the number of active ion channels, variance of ion channel activity and periods when ion channels are inactive (Kirschvink and Walker 1985, Walker 2007). For the multidirectional array, the magnetic field direction was set by directly adjusting the parameter ϕ in figure 1(b). In particular, following Walker (2007), earlier works in magnetic sensing and processing (Taylor and Rutkowski 2015, Taylor 2016), and vector addition and motion perception (Wilson 1999, Trappenberg 2010), we cosine weighted the magnetic field intensity. Mathematically, this gives the following:

$$I_i = (\lambda_1 |\vec{B}|) \cos(\theta_i - \phi) + \nu_i \quad (1)$$

where subscript i represents a particular sensor (figure 3(b)), θ_i represents the orientation of a particular sensor (figure 3(b)), I_i represents an input to the network due to a particular sensor and ν_i represents zero mean Gaussian noise with standard deviation of 0.2 (see Taylor (2016) for details).

For the unidirectional array, the magnetic chain angle ϕ' (figure 1(b)) was indirectly set by first adjusting the magnetic field direction ϕ and then using a quadratic equation to relate the magnetic field direction ϕ to the chain angle ϕ' (see Taylor (2016) for details). Mathematically, this gives the following:

$$I_i = (\lambda_2 |\vec{B}|) \cos(\phi') + \nu_i \,. \quad (2)$$

As is the case in equation (1), I_i represents an input to the network due to a particular sensor and ν_i represents zero mean Gaussian noise with standard deviation of 0.2.

In both the multi and unidirectional simulated sensor arrays, 24 sensors were used. For the multidirectional array, this corresponds to the sensors being spaced apart in 15° increments. Examples of equations (1) and (2) are plotted in figures 5(a) and (c).

For the hardware sensor array, data were obtained from a distributed magnetic sensor array, which is a hardware instantiation of one of the shaded unidirectional patches in figure 3(b). The array consists of eight HMC6352 digital compasses that are connected to an Arduino Mega board via the inter-integrated circuit (I2C) protocol. Each compass provides raw planar magnetic vector data resolved into its own body axes and a processed heading value. For all experiments, magnetic data from the axis of the sensor that was perpendicular to the circle of figure 3(b) was used (i.e. the directions of the outward pointing blue arrows on the circle and the direction of the solid black filled arrows on each unidirectional sensor patch). The other axis and the processed heading data were ignored (see section 5.3 for a discussion of the consequences and possibilities of this choice). To obtain unidirectional data, a single unidirectional sensor patch (figure 3(b)) was used as-is in one orientation. To obtain multidirectional data, the sensor was used in eight angular orientations spaced 45° apart (figure 3(b)). Data were then post-processed in batch to effectively use 64 different sensors that span a full revolution.

We assume that the compasses are sufficiently spaced from each other and associated wiring so that an individual compass' effect on the magnetic field does not interfere with the measurements of the other compasses. In the hardware setup, the wires that connect to the sensors are approximately 1.3 mm from the sensor and the maximum current draw of the sensors is 10 mA according to the sensor datasheet. Based on this information, the magnetic field due to an infinite wire with this current and distance from the sensor is approximately 15 milligauss (Halliday *et al* 2003). This is approximately 3% of Earth's approximately 500 milligauss magnetic field (Johnsen and Lohmann 2005) and 15% of our smallest magnetic field of 100 milligauss. While these effects are small, and thus not considered here for simplicity, future engineering designs must account for them. In animals, when magnetoreceptors are finally identified with certainty, investigating these effects of individual magnetoreceptors on each other will also be of interest.

2.3. Experiments

We conducted several experiments to verify the predictions made in Walker (2007). These experiments are an evolution of the simulation experiments of Taylor (2016). In this section, we outline the experiments that were conducted and analysis methods used for both the multidirectional and unidirectional sensor arrays. We also outline the protocols that were used for experiments in simulation and in hardware.

2.3.1. Weber's law experiment

For both the multidirectional and unidirectional arrays, we held the magnetic field's direction constant while changing its intensity. We then fit linear, logarithmic and power curves to the resulting data to verify whether our results are consistent with Weber's law. To analyze the output of the unidirectional array, the mean activity across all populations was taken at a point in time when the stimulus was active and the network had evolved to a steady state. The mean values were then plotted against their respective intensities. To analyze the output of the multidirectional array, we examined the shape of the neural field output in response to different magnetic field inputs. It was noted from preliminary data that increased magnetic intensity (i.e. increased input) led to the shape of the output being more step-like, with sections where the output is constant and flat, and changes that are sharp as one moves across the neural population nodes (figures 4(a) and 5). This type of output resembles a binary or 'all-or-nothing' response versus a smoother and more curved neural output that occurs in response to a smaller magnetic intensity input (figure 4(c)).

To quantify these differences in output shape, a histogram of the output was made at a point in time when the stimulus was active and the network activity had evolved to a steady state (figures 4(b) and (c)). The number of points in the upper tail was recorded and normalized by the total number of sensors in the neural field. Because this approach quantifies the shape of the neural output, specifically how flat certain sections of the output are, (see figure 4), we refer to this measure as a 'flatness index' or

$$\text{flatness index} = \frac{\text{number of elements in upper tail}}{\text{total number of neurons}}. \quad (3)$$

A large flatness index (i.e. a more step-like and less curved shape, as in figure 4(a)) indicates a strong magnetic field intensity. A small flatness index (i.e. a less step-like and more curved shape, as in figure 4(c)) indicates a weak magnetic field intensity. Plotting the flatness indices against their respective intensities allows us to probe whether or not our model follows Weber's law through either power, or logarithmic relationships. This analysis effectively looks for the proportion of neural populations that exhibit a maximal response, information that a nervous system would be capable of encoding. If multiple neural populations synapse onto a single neural population, the downstream population could be tuned so that it only fires when it receives signals from a sufficient number of upstream neural populations above a given threshold (figures 4(b), (d) and (e)). For example, if a downstream population required that seven upstream populations fired strongly (figure 4(e)), the strong response in figures 4(a) and (b) would satisfy this requirement (top tail is in the 'above threshold' regime), while the weaker response in figures 4(c) and (d) would not (top tail does not reach the 'above threshold' regime). This measure differs from the flatness measure used by Taylor (2016), which used the sum of the two exterior bins. Essentially, Taylor (2016) quantified performance by analyzing both inactive and active neurons, while the present study quantifies performance using only neurons that are active. Analyzing only the active neurons may be more biologically relevant when considering the effects of a set of neural populations on a downstream population (e.g. figure 4(e)).

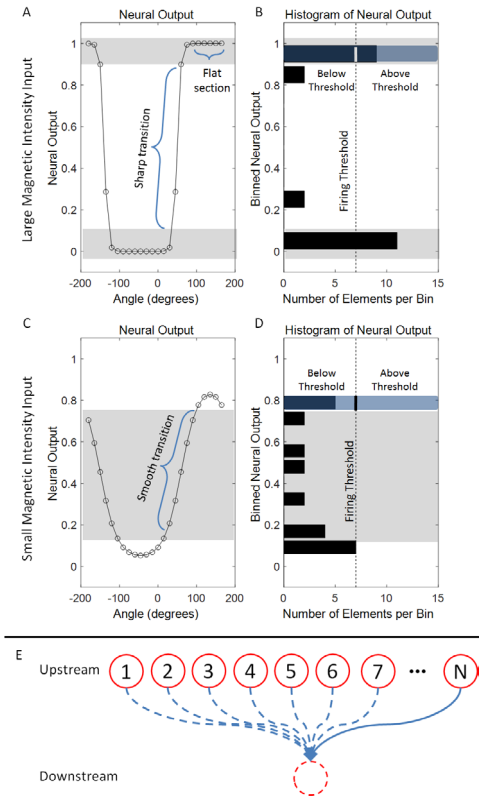

Figure 4. Illustration of how the shape of the output distribution is analyzed for its 'flatness'. Panels (a) and (c) show neural output for one point in time for $\lambda_1|\vec{B}|$ values of 10 and 1, respectively. Panels (b) and (d) show histograms for these outputs. In the case of the stronger magnetic intensity input, most of the data lies in the outer tails of the histogram (light gray bars in panels (a) and (b)). This is in contrast to a smaller magnetic intensity input, where the data are more evenly distributed (light gray bar in panels (c) and (d)). Data used for the flatness index are indicated by the dark blue bar in panels (b) and (d). In panels (a) and (c), the horizontal axis denotes the angle that each node in the network is sensitive to. In panels (b) and (d), the vertical line denotes the number of neural populations that must be in the top tail to elicit a response from a downstream population. The bold vertical line is meant to emphasize whether the top tail has enough neural populations to elicit a downstream response. Panel (e) illustrates how a given number of upstream neural populations could elicit a response from a downstream neural population. In this illustration, the connections between the populations are all the same (i.e. all inhibitory or all excitatory), but only connections one through four are active. Suppose that the downstream population only responds when seven or more of the upstream populations are active. As depicted, at least three more upstream populations must become active to elicit a response from the downstream population.

2.3.2. *Field rotation experiment*

In addition to the experiment with a unidirectional array, we held the intensity of the field constant, but changed its direction relative to the preferred direction of the sensors in the array. The goal was to determine whether a change of direction in the field would result in sensory difference similar to those expected when the intensity of the field changes (prediction 2 from section 1 and (Walker 2007)).

2.3.3. *Simulation experiment protocol*

For the simulation experiments, the intensity and direction of the magnetic field were altered by changing the magnetic field intensity parameters $\lambda_1|\vec{B}|$ and $\lambda_2|\vec{B}|$, and magnetic direction ϕ (equations (1) and (2), and figures 1 and 3). The magnetic field intensity parameter for the multidirectional array Weber's law experiment ($\lambda_1|\vec{B}|$) was set to the following values: 0.1, 0.5, 1.0, 2.0, 3.0, 4.0, 5.0, 6.0, 7.0, 8.0, 9.0 and 10.0. For the unidirectional array Weber's law experiments, the magnetic field intensity parameter ($\lambda_2|\vec{B}|$) was set to the following values: 0.5, 1.0, 1.5, 2.0, 2.5, 3.0, 3.5, 4.0, 7.0 and 10.0. For the field rotation experiment, for a fixed magnetic field intensity $\lambda_2|\vec{B}| = 2$, the value of ϕ was varied from $0° - 25°, 80° - 100°$ and $155° - 180°$. Each block of angles was varied in $5°$ increments.

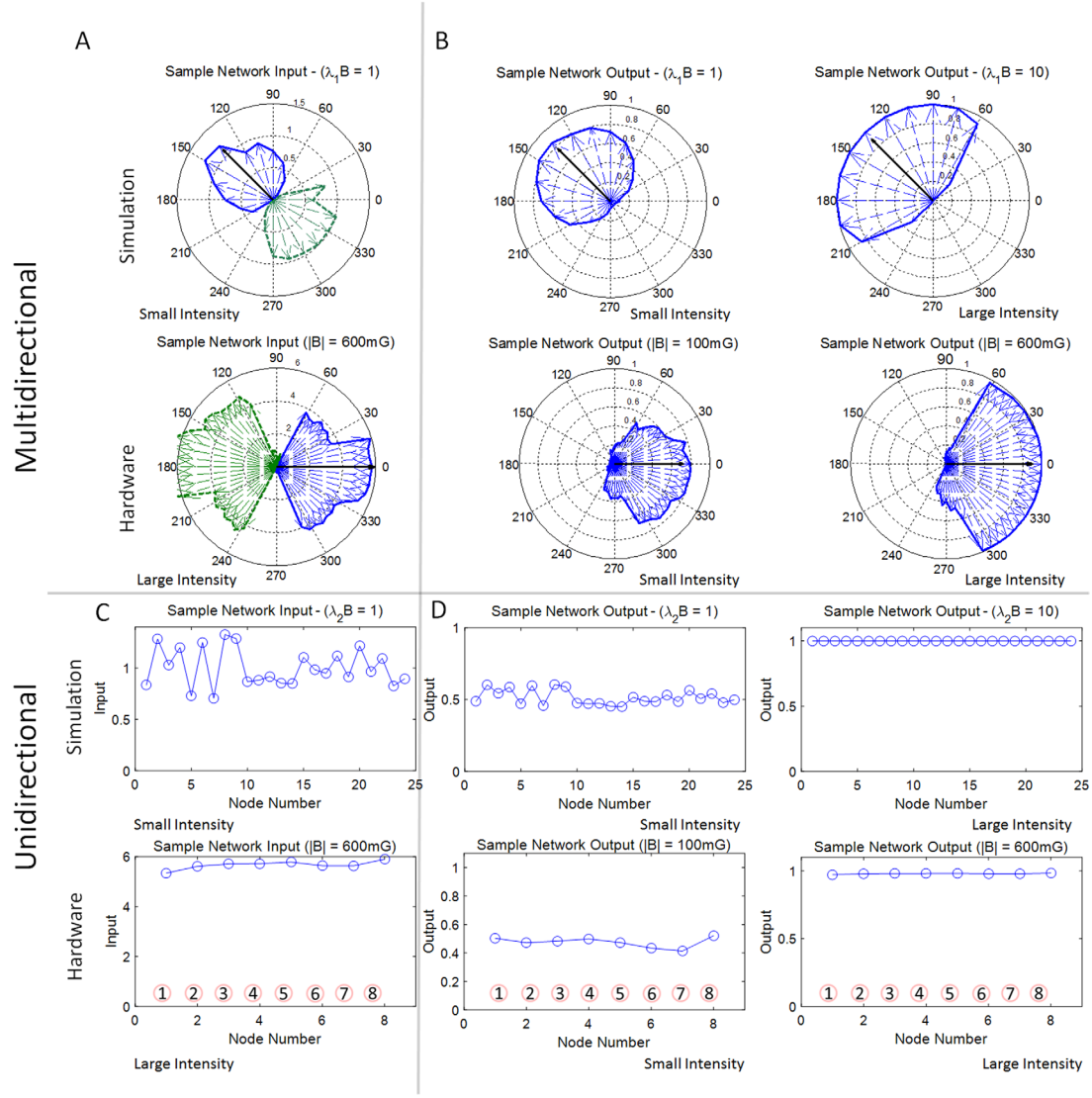

Figure 5. Sample input ((a) and (c)) and output ((b) and (d)) data from the multidirectional and unidirectional sensor arrays, respectively. In panel A, blue areas outlined by the solid blue line denote positive input values and green areas outlined by the dashed green line denote negative input values. In panels (a) and (b) (plotted in polar coordinates), the black arrow denotes the direction of the applied magnetic field. Outputs are shown for both large and small intensity inputs. In panels (a) and (c), the simulation plots are graphical examples of equations (1) and (2), respectively. In panels (c) and (d), the red numbered circles are graphical depictions of unidirectional sensor array nodes (see figures 3(a) and 4(e)).

2.3.4. Hardware experiment protocol

For the hardware experiments, the magnetic field was manipulated using a three-coil artificial magnetic environment at the University of North Carolina at Chapel Hill. Each of the three coils was based on the design of Alldred and Scollar (1967). A Sparton AHRS 8 attitude/heading/reference system was used to provide a truth reference regarding the state of the magnetic field inside of the artificial magnetic environment. The coil aligned with the vertical component of the field was used to cancel this component so that the resultant magnetic field was horizontal (i.e. perpendicular to the gravity vector). For the multidirectional array Weber's law experiments, the magnetic intensity was varied through the following values (all in milligauss): 100, 200, 300, 400, 500 and 600. For the unidirectional array Weber's law experiments, the magnetic field intensity was varied through the following values (all in milligauss): 50, 100, 150, 200, 238, 250, 300, 350, 400, 450, 500, 550 and 600. For the magnetic field rotation experiment, at a constant magnetic field intensity of approximately 251 milligauss, the magnetic field angle was varied through the following angles (all in degrees): 2.2, 10.7, 15.7, 20.6, 25.5, 30.5, 85.4, 90.4, 95.7, 100.5 and 105.7. Angles greater than 105.7° were not used due to the power limitations of the coil system.

2.4. Experimental predictions

Although section 2.3 was organized on the basis of the different experiments and protocols, different analysis methods are required for the multidirectional and unidirectional sensor arrays. Therefore, both our experimental predictions and results are organized on the basis of sensor array type in the following sections.

2.4.1. Multidirectional predictions (Weber's law experiment)

Figure 5(a) shows sample simulated and hardware inputs into the multidirectional sensor array. In particular, the simulated input is a graphical example of equation (1). For the multidirectional array, based on the sample input data and the results of Taylor (2016), we predicted that the flatness index should vary logarithmically with the magnetic intensity for both the simulation and hardware experiments. It is possible that a power law may apply.

2.4.2. Unidirectional predictions (Weber's law and field rotation experiments)

Figure 5(c) shows sample simulated and hardware inputs into the unidirectional sensor array. In particular, the simulated input is a graphical example of equation (2). For the unidirectional array, provided that the hardware sensors receive magnetic field information that is predominantly aligned with the sensor's queried direction (see figure 3(b)), one would expect the neural output to vary logarithmically with the magnetic intensity in both the simulation and hardware experiments (Taylor 2016). It is also possible that a power law may apply. In some limited regime, it is possible that the neural output might vary linearly with the magnetic intensity.

With respect to the field rotation experiment, Taylor (2016) demonstrated that with an appropriate sensor, a magnetic field rotation could result in a membrane potential change. One would expect to see the same type of qualitative behavior in the hardware sensor. However, because the simulated sensor model does not identically mirror the hardware sensors, there may be discrepancies in the resulting system outputs.

2.4.3. Compass considerations

It is important to note that this study only uses one axis of the hardware's compasses and that these outputs can be positive or negative. In contrast, the simulated unidirectional input is only positive and is symmetric about 90° (see Taylor (2016) for a description). Therefore, when the applied field angle is close to zero, the modeled and hardware sensor inputs are qualitatively similar. However, as the applied field angle increases, the simulated sensor input decreases and then begins to increase after the field angle passes 90°. In contrast, the hardware sensor input decreases from a maximum positive number down to a negative number. As a result, we would expect that the neural field responses to a rotated magnetic field in the simulation and the hardware should be qualitatively similar when the magnetic field angle is close to zero. However, they may begin to differ as the field approaches and passes through 90°. Despite this difference in sensing capability, the use of the hardware sensors for this experiment is valuable because it provides a real-world point of comparison for the simulation in a regime where the real and simulated inputs are similar (i.e. near zero degrees).

3. Results

Figure 5 shows example inputs and outputs from the multidirectional (figures 5(a) and (b)) and unidirectional (figures 5(c) and (d)) arrays for both the simulated and hardware sensors. Inputs and outputs from large and small magnetic field intensities illustrate the range of input/output behavior. The input plots (figures 5(a) and (c)) show simulated sensor data (equations (1) and (2)), and real-world sensor data. The output plots show how the shape of the neural output changes as the magnetic field strength increases (larger diameter and arc-length for the multidirectional array, and a more constant output for the unidirectional array). For the multidirectional array, the neural output is geometrically aligned with the direction of the magnetic field.

Figure 6 shows the outputs of the multidirectional and unidirectional arrays plotted against the magnetic intensity, along with various curve fits to different regimes of the data. The R^2 values for all curve fits were greater than or equal to 0.95. These plots provide an insight as to whether the sensory system follows Weber's law (prediction 4 from section 1).

Figure 7 shows the results from varying the magnetic field direction while holding the magnetic field intensity constant for a unidirectional array. This probes the validity of the prediction that rotating the direction of the magnetic field generates a response that is similar to changing its intensity.

4. Discussion

4.1. A multidirectional sensor array detects field direction and intensity, and follows Weber's law

Figure 5(b) shows sample results of detecting and processing magnetic field data with a multidirectional array. In both the simulated and hardware experiments, as the field intensity increases, so does the flatness index of the neural field response (figures 6(a) and (b)). The increase in flatness index is indicative of the neural output having a more step-like shape, as shown in figure 4(a). Combined with the spatial distribution of neural output (figure 5(b)), the results demonstrate that this approach can successfully encode both the direction and magnitude of the field. Figures 6(a) and (b) shows that the neural response saturates for higher magnetic field intensity values. It also shows that the neural field approach yields results that are consistent with Weber's law. For both the simulated and hardware experiments, the neural responses to lower and mid-level magnetic field intensities follow a linear trend, while the response to all intensities loosely follows power and logarithmic trends.

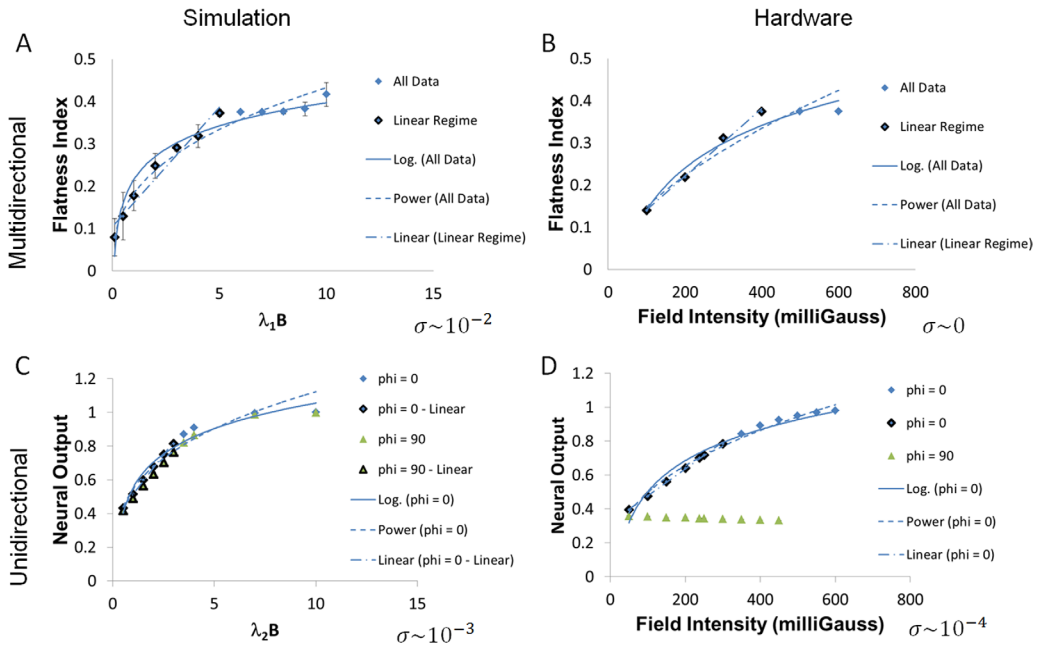

Figure 6. Output data from the multidirectional ((a) and (b)), and unidirectional ((c) and (d)) arrays for varying intensity. Panels (a) and (b) show the flatness index, while panels (c) and (d) show the mean neural output level. Logarithmic, power and linear fits were performed for each set of data. Linear fits were only performed on the regions of data titled 'Linear'. Phi refers to the magnetic field direction ϕ in figure 1. σ refers to the order of magnitude of error bars (standard deviation) in each plot. Because of the orientation of the magnetic field relative to the multidirectional hardware setup, the results came out the same for each trial, hence a σ value of 0.

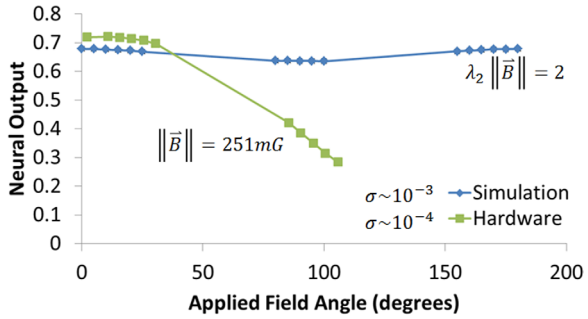

Figure 7. Results from varying the external field direction in both the simulated and hardware experiments. Data was taken for low (0° to 20°), mid-size (80° to 100°) and large (155° to 180°) magnetic field angles. For the hardware experiments, the field was not rotated past 100 degrees due to power limitations of the artificial magnetic environment. σ refers to the order of magnitude of error bars (standard deviation) for each curve, which are not visible due to their relatively small size. Each data point represents the mean of 100 simulation trials and 20 hardware trials.

4.2. A unidirectional sensor array detects field intensity and follows Weber's law

Figure 5(d) shows sample results of detecting and processing magnetic field data with a unidirectional array. For both the simulation and hardware experiments, when the field is oriented with the preferred direction of the sensors, the output follows Weber's law (figures 6(c) and (d)). For the hardware results, when the field is rotated 90°, the neural output becomes constant. The reason for the discrepancy between this result and that of the simulated data is that the modeled input (based on theory) in this regime does not match how the engineered hardware sensors work. The hardware sensors detect the component of the magnetic field pointing in their preferred direction. If a magnetic field is orthogonal to this preferred direction, the sensor will output a constant baseline value and increasing or decreasing the field strength will have a marginal effect at best. In contrast, the simulated input was constructed such that there would be a non-constant baseline output regardless of the magnetic field's orientation. This point can be further seen by examining figure 7. As can be seen, while the hardware and simulation results qualitatively match in their trends up to 90°, the hardware response does not rebound after 90° of magnetic field rotation, but instead continues to drop. If the field direction were further rotated, the hardware response would continue to decrease and reach a minimum near zero. Regardless of this difference, figure 7 shows consistency between the hardware and simulation experiments in terms of nearest-neighbors exhibiting nearly identical behavior

and more distant neighbors exhibiting different behavior. In figure 7, for the hardware portion of the experiment, the field was not rotated farther than 100° due to power limitations of the artificial magnetic environment.

5. Conclusion

5.1. Overview

Through simulation and hardware experimentation, our work demonstrates the plausibility of the predictions posed by Walker's theoretical model (Walker 2007). Additionally, our results demonstrate that dynamic neural fields are a viable way to process sensory data from a distributed set of magnetic sensors. We believe that by using neural fields as a processing mechanism, our work can be extended to process data from other sensor modes that employ a distributed sensing paradigm. This would offer a tool that can be used to both study sensory biology questions and also to push the boundaries of advanced and robust sensing and processing in engineered systems.

5.2. Biology applications and insights

The results of our analyses, both in terms of simulations and hardware measurements, give credence to the hypothesis that field intensity can be detected using an array of multiple sensors, each of which primarily detects field direction. Of course, whether the ability of animals to detect magnetic field intensity is actually based on a similar mechanism is unknown. In this context, however, an interesting speculation is that animals might first have evolved single receptors that functioned to detect the direction of the magnetic field. Subsequently, in the course of evolution, a single receptor might have given rise to multiple receptors, which in turn became integrated into a functional unit that can detect intensity.

Regardless of these considerations, the approach presented in the study provides a versatile methodology that can be used to make predictions and aid in analyses of diverse mechanisms of animal magnetoreception. For example, the input to the neural field model can be modified to work with potential sensing mechanisms other than magnetite, such as the cryptochrome-based radical pair mechanism (Ritz *et al* 2000, Mouritsen *et al* 2004, Johnsen and Lohmann 2005, 2008, Reppert *et al* 2010, Wajnberg *et al* 2010, Gegear *et al* 2010, Mouritsen and Hore 2012). In particular, because the radical pair mechanism appears to be especially suitable for functioning as a compass (Mouritsen and Hore 2012), our work suggests that with the right processing, several radical-pair-based sensors may be able to encode both compass information and some amount of intensity information. As research on animal magnetoreception and its neural underpinnings continues, the approach used in this study can be modified to reflect new information and used to evaluate new hypotheses.

5.3. Engineering applications

In addition to generating biological insights, this study can have several direct engineering impacts. For example, as mentioned in section 2.2, only one of the axes on each sensor was used in processing the magnetic signal. However, by appropriately aggregating and processing this single quantity over several sensors that have different orientations, both intensity and direction were encoded. One could envision applying this to sensing on mobile platforms. If the processing can be done at an appropriate rate, then it might be possible to obtain magnetic information through a distributed array of unidirectional sensors that are each oriented differently. This kind of system may have advantages over a traditionally built system, including reduced cost (using many inexpensive sensors versus using one or a few high-precision sensors) and graceful degradation with sensor malfunction (as opposed to catastrophic failure for a system dependent on one or a few sensors). Additionally, Taylor and Rutkowski (2015) showed that this type of sensing and processing paradigm might be able to indirectly provide information regarding system health and reliability (e.g. how many sensors have failed, sensor data integrity). Also, this paradigm may not be limited to magnetoreception. If the sensor mode in question can be appropriately fed to a dynamic neural field, then similar approaches can be used to process data from a variety of sensor modes and even process data from multiple sensing modes (Taylor and Rutkowski 2015). This kind of distributed sensing approach appears in several animal sensory systems such as strain-detecting Campaniform sensilla (Zill *et al* 2004), skin (Dargahi and Najarian 2004) and cricket cerci (Jacobs *et al* 2008). The neural field approach may provide a path to using distributed sensing in engineered systems. In particular, with the advent of new manufacturing techniques, one could envision eventually building a distributed sensor (e.g. a field of strain detectors) directly into a mobile platform for proprioceptive (i.e. onboard) and exteroceptive (i.e. offboard) feedback.

5.4. Future directions

Several steps can be taken to advance this work. In particular, this study assumes only one type of weighting function and that the network is fully connected such that there is a periodicity in the connections. This only represents one kind of possible neural topology. Both non-fully-connected and non-periodic topologies are possible (e.g. Wilson (1999)). Additionally, there are other types of networks and dynamics, such as Wilson–Cowan cortical dynamics and winner-take-all networks (Wilson and Cowan 1973, Wilson 1999). Future work can explore the consequences of using different neural topologies by using different types of weighting functions and different types of networks. For example, the winner-take-all network described by

Wilson (1999) only allows a fixed number of nodes to become active in response to a stimulus and parabolic interpolation of these nodes can allow the network to accurately encode information about the input (Wilson *et al* 1992).

We note here that using different types of network topologies may necessitate the use of different analysis tools and performance metrics. For example, with the network and topology used in this study, the flatness index provided insight into the behavior of the system. However, if Wilson–Cowan dynamics are used, the neural output may be a narrow band or pair of bands (Wilson 1999). In this case, the flatness index would not be a sensible performance measure. Future studies could focus on modifying the flatness index presented here. For example, one could envision weighting the proportion of populations in the top tail by the average activity of the populations in the top tail. Additionally, different metrics can be developed that would apply to other network topologies and constructions. Also, metrics could be developed that attempt to understand the activity of a population relative to the dynamic ranges of its constituent neurons. From a biology perspective, as the research community learns more about the neural mechanisms underlying magnetoreception, analysis tools specific to these mechanisms can be developed. From an engineering standpoint, developing a number of analysis tools would be beneficial in terms of applying an appropriate network topology and construction to a given use case.

Additionally, future studies can focus on implementing the neural field approach in real-time and using it to process magnetic and multimodal sensor data for actively navigating mobile platforms. This would allow for both engineered prototyping and biological hypothesis testing. As an example, Szczecinski (2013) explored implementing central pattern generators on a field programmable gate array to explore hardware implementation of neuromorphic legged locomotion control. In addition, advances such as IBM's TrueNorth neuromorphic chip (Hsu 2014) present interesting opportunities to expand on the work presented in this study. Beyond these efforts, future works can focus on expanding the current study to sensors that point in all three dimensions (i.e. a sphere) versus covering a single plane (i.e. a circle).

From an engineering standpoint, it would be interesting to investigate the potential overlap between the neural field approach and more standard estimation techniques such as Kalman and particle filters (e.g. Crassidis and Junkins (2012); Gelb (1974)). It may also prove fruitful to explore the potential overlap between the neural field approach and other data acquisition and processing methods such as compressive sensing (Candes and Wakin 2008). Previous work showed that the neural field approach may be able to provide near optimal results (Taylor and Rutkowski 2015) and there is an exciting intersection between engineered control and estimation methods, and computational neuroscience (Schiff 2012).

From a biological magnetoreception standpoint, the neural field approach may prove valuable for research into the magnetite-based mechanism and other hypothesized magnetosensory mechanisms, such as the light-mediated radical pair hypothesis. It would also be interesting to use the neural field approach to investigate how directional sensors might evolve into an ensemble of functional units that detect both direction and intensity.

Acknowledgments

The authors thank Mr Stephen Card (AFRL/RWWN) for assistance in designing and building the distributed magnetic sensor. They also thank Dr Jennifer Talley and Mr Ric Wehling (AFRL/RWWI), and Mr Sergio Cafarelli (MacCauly Brown) for assistance in editing the manuscript.

Funding

This work was supported in part by a Visiting Scientist Program award from the Air Force Office of Scientific Research. The work was also supported in part by a grant from the Air Force Office of Scientific Research (Grant FA9550-14-1-0208). Opinions expressed here are not necessarily those of the United States Air Force, Air Force Research Laboratory, Air Force Office of Scientific Research, or Department of Defense.

References

Alldred J C and Scollar I 1967 Square cross section coils for the production of uniform magnetic fields *J. Sci. Instrum.* **44** 755–60

Amari S 1977 Dynamics of pattern formation in lateral-inhibition type neural fields *Biol. Cybern.* **27** 77–87

Akre K L and Johnsen S 2014 Psychophysics and the evolution of behavior *Trends Ecol. and Evol.* **5** 291–300

Browning N A, Grossberg S and Mingolla E 2009 Cortical dynamics of navigation and steering in natural scenes: motion-based object segmentation, heading, and obstacle avoidance *Neural Netw.* **22** 1383–98

Boles L C and Lohmann K J 2003 True navigation and magnetic maps in spiny lobsters *Nature* **6918** 60–3

Boxerbaum A S 2012 Continuous wave peristaltic motion in a robot *PhD Dissertation* Case Western Reserve University (http://rave.ohiolink.edu/etdc/view?acc_num=case1333649965)

Candes E J and Wakin M B 2008 An introduction to compressive sampling *IEEE Signal Process. Mag.* **25** 21–31

Coombes S, Graben P B, Potthast R and Wight J 2014 *Neural Fields: Theory and Applications* (Berlin: Springer) (https://doi.org/10.1007/978-3-642-54593-1)

Crassidis J L and Junkins J L 2012 *Optimal Estimation of Dynamic Systems* 2nd edn (Boca Raton, FL: CRC Press)

Dennis T E, Rayner M J and Walker M 2007 Evidence that pigeons orient to geomagnetic intensity during homing *Proc. R. Soc.* B **274** 1153–8

Dargahi J and Najarian S 2004 Human tactile perception as a standard for artificial tactile sensing—a review *Int. J. Med. Robot. Comput. Assist. Surg.* **1** 23–35

Edelman N B *et al* 2015 No evidence for intracellular magnetite in putative vertebrate magnetoreceptors identified by magnetic screening *Proc. Natl Acad. Sci.* **112** 262–7
Eder S H K, Cadiou H, Muhamad A, McNaughton P A, Kirschvink J L and Winklhofer M 2012 Magnetic characterization of isolated candidate vertebrate magnetoreceptor cells *Proc. Natl Acad. Sci.* **109** 12022–7
Gegear R, Foley L, Casselman A and Reppert S 2010 Animal cryptochromes mediate magnetoreception by an unconventional photochemical mechanism *Nature* **463** 804–7
Gelb A *et al* 1974 *Applied Optimal Estimation* (Cambridge, MA: MIT Press)
Gould J L 1982 The map sense of pigeons *Nature* **296** 205–11
Grossberg S 1973 *Contour Enhancement, Short Term Memory, and Constancies in Reverberating Neural Networks* (*Studies in Applied Mathematics* vol 52) (Dordrecht: Springer) pp 213–57
Halliday D, Resnick R and Walker J 2003 *Fundamentals of Physics* vol 2, 6th edn (New York: Wiley)
Hsu J 2014 IBM's new brain *IEEE Spectr.* **51** 17–9
Jacobs G A, Miller J P and Aldworth Z 2008 Computational mechanisms of mechanosensory processing in the cricket *J. Exp. Biol.* **211** 1819–28
Jensen K K 2010 Light-dependent orientation responses in animals can be explained by a model of compass cue integration *J. Theor. Biol.* **262** 129–41
Johnsen S and Lohmann K J 2005 The physics and neurobiology of magnetoreception *Nat. Rev. Neurosci.* **6** 703–12
Johnsen S and Lohmann K J 2008 Magnetoreception in animals *Phys. Today* **61** 29–35
Kandel E R and Schwartz J H 1981 *Principles of Neural Science* (New York: Elsevier)
Kandel E R, Schwartz J H and Jessell T M 2000 *Principles of Neural Science* 4th edn (New York: McGraw-Hill)
Kirschvink J L, Dizon A E and Westphal J A 1986 Evidence from strandings for geomagnetic sensitivity in cetaceans *J. Exp. Biol.* **120** 1–24
Kirschvink J L and Walker M M 1985 Particle-size considerations for magnetite-based magnetoreceptors *Magnetite Biomineralization and Magnetoreception in Organisms: a New Biomagnetism* ed J L Kirschvink *et al* (New York: Plenum)
Klimley A P 1993 Highly directional swimming by scalloped hammerhead sharks *Sphyrna lewini*, and subsurface irradiance, temperature, bathymetry, and geomagnetic field *Mar. Biol.* **117** 1–22
Klinowska M 1985 Cetacean live stranding sites relate to geomagnetic topography *Aquatic Mammals* **1** 27–32
Knecht D J and Shuman B M 1985 The geomagnetic field *Handbook of Geophysics and the Space Environment* ed A Jursa (Washington, DC: Air Force Geophysics Laboratory)
Lohmann K J and Lohmann C M F 1996 Detection of magnetic field intensity by sea turtles *Nature* **380** 59–61
Lohmann K J, Hester J T and Lohmann C M F 1999 Long-distance navigation in sea turtles *Ethol. Ecol. Evol.* **11** 1–23
Lohmann K J, Lohmann C M F, Ehrhart L M, Bagley D A and Swing T 2004 Animal behaviour: geomagnetic map used in sea-turtle navigation *Nature* **428** 909–10
Lohmann K J, Lohmann C M F and Putman N F 2007 Magnetic maps in animals: nature's GPS *J. Exp. Biol.* **210** 3697–705
Lohmann K J, Putman N F and Lohmann C M F 2012 The magnetic map of hatchling loggerhead sea turtles *Curr. Opin. Neurobiol.* **22** 336–42
Mouritsen H, Janssen-Bienhold U, Liedvogel M, Feenders G, Stalleicken J, Dirks P and Weiler R 2004 Cryptochromes and neuronal-activity markers colocalize in the retina of migratory birds during magnetic orientation *Proc. Natl Acad. Sci.* **101** 14294–9
Mouritsen H and Hore P 2012 The magnetic retina: light-dependent and trigeminal magnetoreception in migratory birds *Curr. Opin. Neurobiol.* **22** 343–52
Putman N F, Scanlan M M, Billman E J, O'Neil J P, Couture R B, Quinn T P, Lohmann K J and Noakes D L G 2014 An inherited magnetic map guides ocean navigation in juvenile Pacific salmon *Curr. Biol.* **24** 446–50
Ritz T, Adem S and Schulten K 2000 A model for photoreceptor-based magnetoreception in birds *Biophys. J.* **78** 707–18
Reppert S M, Gegear R J and Merlin C 2010 Navigational mechanisms of migrating monarch butterflies *Trends Neurosci.* **33** 399–406
Schiff S J 2012 *Neural Control Engineering. Computational Neuroscience* ed T J Sejnowski and T A Poggio (Cambridge, MA: MIT Press)
Shaw J, Boyd A, House M, Woodward R, Falko M, Cowin G, Saunders M and Baer B 2015 Magnetic particle-mediated magnetoreception *J. R. Soc.: Interface* **12** 20150499
Shepherd G M 1994 *Neurobiology* 3rd edn (New York: Oxford University Press)
Skiles D D 1985 The geomagnetic field: its nature, history, and biological relevance *Magnetite Biomineralization and Magnetoreception in Organisms: a New Biomagnetism* ed J L Kirschvink *et al* (New York: Plenum)
Szczecinski N 2013 Massively distributed neuromorphic control for legged robots modeled after insect stepping *MS Thesis* Case Western Reserve University (http://rave.ohiolink.edu/etdc/view?acc_num=case1354648661)
Szczecinski N S, Brown A E, Bender J A, Quinn R D and Ritzmann R E 2013 A neuromechanical simulation of insect walking and transition to turning of the cockroach *Blaberus discoidalis Biol. Cybern.* **108** 1–21
Taylor B K 2016 Validating a model for detecting magnetic field intensity using dynamic neural fields *J. Theor. Biol.* **408** 53–65
Taylor B K and Rutkowski A J 2015 Bio-inspired magnetic field sensing and processing *Proc. Institute of Navigation's Pacific PNT Conf.*
Trappenberg T P 2010 *Fundamentals of Computational Neuroscience* 2nd edn (New York: Oxford University Press)
Vidal-Gadea A *et al* 2015 Magnetosensitive neruons mediate geomagnetic orientation in *Caenorhabditis elgans eLife* **4** e07493
Wajnberg E, Acosta-Avalos D, Alves O C, de Oliveria J F, Srygley R B and Esquivel D M S 2010 Magnetoreception in eusocial insects: an update *J. R. Soc.: Interface* **7** S207–25
Walker M 2007 A model for encoding of magnetic field intensity by magnetite-based magnetoreceptor cells *J. Theor. Biol.* **250** 85–91
Walker M 1998 On a wing and a vector: a model for magnetic navigation by homing pigeons *J. Theor. Biol.* **192** 341–9
Wilson H and Cowan J D 1973 A mathematical theory of the functional dynamics of cortical and thalamic nervous tissue *Kybernetik* **13** 55–80
Wilson H, Ferrera V P and Yo C 1992 A psychophysically motivated model for two-dimensional motion perception *Vis. Neurosci.* **9** 79–97
Wilson H 1999 *Spikes, Decisions, and Actions: the Dynamical Foundations of Neuroscience* (New York: Oxford University Press)
Wiltschko R and Wiltschko W 1995 *Magnetic Orientation in Animals* (Berlin: Springer)
Wiltschko R and Wiltschko W 2013 The magnetite-based receptors in the beak of birds and their role in avian navigation *J. Comparative Physiol.* A **199** 89–98
Wu L-Q and Dickman J D 2012 Neural correlates of a magnetic sense *Science* **336** 1054–7
Yorke E D 1985 Energetics and sensitivity considerations of ferromagnetic magnetoreceptors *Magnetite Biomineralization and Magnetoreception in Organisms: a New Biomagnetism* ed J L Kirschvink *et al* (New York: Plenum)
Zhang K 1996 Representation of spatial orientation by the intrinsic dynamics of the head-direction cell ensemble: a theory *J. Neurosci.* **16** 2112–26
Zill S, Schmitz J and Bűschges A 2004 Load sensing and control of posture and locomotion *Arthropod Struct. Dev.* **33** 273–86